Spin-glass-like properties of $La_{0.8}Ca_{0.2}MnO_3$ nanoparticles ensembles

V. Markovich,[1,*] I. Fita,[2,3] A. Wisniewski,[2] G. Jung,[1] D. Mogilyansky,[4] R. Puzniak,[2] L. Titelman,[4] and G. Gorodetsky[1]
[1]*Department of Physics, Ben-Gurion University of the Negev, P.O. Box 653, 84105 Beer-Sheva, Israel*
[2]*Institute of Physics, Polish Academy of Sciences, Aleja Lotnikow 32/46, 02-668 Warsaw, Poland*
[3]*Donetsk Institute for Physics & Technology, National Academy of Sciences, 83114 Donetsk, Ukraine*
[4]*Institute of Applied Research, Ben-Gurion University of the Negev, 84105 Beer-Sheva, Israel*
(Received 8 December 2009; revised manuscript received 14 March 2010; published 30 April 2010)

Magnetic properties of compacted $La_{0.8}Ca_{0.2}MnO_3$ manganite nanoparticles with average particle size of 18 and 70 nm and Curie temperatures $T_C \approx 231$ K and $T_C \approx 261$ K, respectively, have been investigated. The relative volume of the ferromagnetic phase has been estimated to be 52% for ensembles of 18 nm particles and 92% for 70 nm particles. It was found that applied hydrostatic pressure enhances T_C of $La_{0.8}Ca_{0.2}MnO_3$ nanoparticles at a rate $dT_C/dP \approx 1.8-1.9$ K/kbar, independently on the average particle size. Pronounced irreversibility of magnetization below $T_{irr} \approx 208$ K and strong frequency dependent ac susceptibility below T_C for smaller 18 nm particles have been observed. 18 nm particles have also shown aging and memory effects in zero-field-cooled (ZFC) and field-cooled magnetization. These features indicate the appearance of spin-glass-like state, partially reminiscent the behavior of $La_{1-x}Ca_xMnO_3$ crystals, doped below the percolation threshold $x < x_C = 0.225$. In contrast, ensembles of larger 70 nm particles have shown insignificant irreversibility of magnetization only and no frequency dependence of ac susceptibility, similarly to the behavior of $La_{1-x}Ca_xMnO_3$ crystals with $x > x_C$. The temperature of the ZFC magnetization maximum for 18 nm particles decreases with increasing magnetic field and forms a critical line with an exponent 1.89 ± 0.56. The results suggest that superspin-glass features in ensembles of interacting 18 nm particles appear along with superferromagnetic-like features.

DOI: 10.1103/PhysRevB.81.134440 PACS number(s): 75.47.Lx, 75.50.Tt, 75.50.Lk

I. INTRODUCTION

Nanosized materials, such as nanoparticles (NPs), nanowires, nanotubes, and nanocomposites are currently a focus of intense investigations. When the size of NPs is reduced to the nanometer scale, some of the basic magnetic properties become strongly size dependent and differ significantly from the properties of the bulk material.[1–6] Ensembles of NPs with weak interparticle magnetic interactions show *superparamagnetic* (SPM) behavior. Systems with pronounced interparticle interactions exhibit collective behavior capable of overcoming anisotropic properties of individual particles. Strongly interacting and dense NP systems showing spin-glass (SG) behavior are referred to, by analogy with atomic spin glasses in bulk materials, as *superspin glasses* (SSG).[6,7] SSG NP systems exhibit peculiar slow dynamics, aging, rejuvenation phenomena, and memory effects.[8–13] NP ensembles at higher densities and stronger interparticle interactions convert into so-called *superferromagnetic* (SFM) state in which, below some temperature, the magnetic moments of all NPs are correlated in a ferromagnetic-like fashion.[14,15]

In recent years, a plethora of unusual nonequilibrium dynamics and time-dependent phenomena in phase-separated perovskite manganites have been reported.[16–20] In particular, relaxation and memory effects in magnetization and resistivity, irreversibility of magnetization, frequency-dependent ac susceptibility, aging, and rejuvenation, similar to those observed in classical spin glasses, were detected in colossal magnetoresistance manganites.[16–21] On the other hand, the glassy behavior in phase-separated manganites is strongly connected with the dynamical coexistence of magnetically distinct phases[16–21] and therefore, manganites do not behave like canonical spin glasses.[22] In manganites, the most important prerequisites for the spin-glass-like behavior, frustration, and disorder are caused by competing interactions together with the phase separation associated randomness in spin positions. Since the dominant interactions leading to frustration appear between nanosized phase-separated clusters, the glassy state in manganites is referred to as a cluster spin glass, see (Ref. 21) and references therein.

A rich variety of phenomena resembling spin/cluster glass effects was found in low-doped ferromagnetic $La_{1-x}Ca_xMnO_3$ for x below the percolation threshold $x_C = 0.225$. In particular, neutron diffraction,[23] NMR,[24] ac susceptibility and dc magnetization,[25] Mössbauer,[26] heat-capacity, and resitivity[25] data, all indicate that bulk $La_{1-x}Ca_xMnO_3$ samples with x close to 0.2 undergo an additional phase transition at temperatures well below the Curie temperature T_C of para-to-ferromagnetic transition. The additional phase transition is accompanied by peculiar features, such as strong frequency dependence of ac susceptibility,[25] remarkable rotation of the easy magnetization axis,[25] wipe-out of the ^{139}La NMR signal upon heating,[24] excess specific heat,[25] and orthorhombicity reduction below the critical point.[23] The ensemble of such features is considered to be a fingerprint of a cluster spin-glass transition in disordered manganites.[21,22] Remarkably, all glass-like features disappear when the doping level x in $La_{1-x}Ca_xMnO_3$ bulk samples approaches and exceeds the percolation threshold x_C.[25]

In this paper, we discuss magnetic and glassy properties of ensembles of $La_{0.8}Ca_{0.2}MnO_3$ (LCMO) NPs with distinct average particle sizes. We show that ensembles of compacted 70 nm NPs do not show any spin-glass features while compacted smaller 18 nm particles exhibit frequency-dependent

ac susceptibility, aging, and memory effects typical for superspin glasses.

II. SAMPLE PREPARATION AND STRUCTURAL CHARACTERIZATION

Nanocrystalline LCMO particles have been prepared by the glycine-nitrate method, similar to that developed for preparation of nanosized $La_{0.7}Ca_{0.3}MnO_3$ powders.[27] A stoichiometric amounts of $La(NO_3)_3 \cdot 6H_2O$, $Ca(NO_3)_2 \cdot 6H_2O$, $Mn(NO_3)_2 \cdot 4H_2O$, and glycine ($C_2H_5NO_2$) were dissolved in water to form precursors solutions. A molar ratio of ~0.5 between glycine and nitrate turned out to be appropriate for producing a single-phase perovskite compound. The precursor solution of each nitrate with glycine was well mixed by 4 h long stirring. The solutions were merged together and mixed again by stirring for another 15 h. The resulting homogenous solution was then dehydrated by heating at $T \sim 100$ °C for 1.5–2 h until it converted into a transparent viscous gel. The gel heated to $T \sim 300$ °C auto ignites and after a short combustion converts into a black porous ash of $La_{0.8}Ca_{0.2}MnO_3$ compound. Upon calcination of the powders for 1 h at 600 °C (900 °C) in the flow of 40% O_2 and 60% Ar, small (large) LCMO nanocrystals are formed. Thus obtained powders were compacted under pressure of 5 kbar into cylinder and pellet shaped samples for magnetic and transport measurements, respectively. The density of the compacted material was about 60% of the density of the bulk crystal.

The NPs were characterized by x-ray powder diffraction (XRD) and transmission electron microscope (TEM) equipped with energy-dispersive x-ray spectroscopy (EDS) facilities. The XRD data were collected by means of powder diffractometer, with a graphite monochromator on diffracted beam providing K_α radiation ($\lambda = 1.541$ Å) and operating at $V = 40$ kV and $I = 30$ mA. The XRD pattern of the as-prepared sample was found to be a mixture of perovskite and amorphous phases. After annealing at $T \sim 600$ °C, pure orthorhombic structure definitely dominates and only a small amount of amorphous phase was detected. The XRD patterns of the samples calcinated at 600 and 900 °C are shown in Fig. 1(a). The diffraction peaks were indexed in the orthorhombic setting of the *Pnma* space group.

The EDS analysis confirmed the composition and homogeneous distribution of the constituent elements. The average composition obtained from EDS spectra recorded at different areas agrees well with the starting composition in terms of the atomic ratio, La:Ca:Mn=0.8:0.2:1.0. To determine the lattice parameters and crystallite sizes the Rietveld analysis of XRD spectra was performed using the FULLPROF computer tool.[28] The Rietveld plot for the sample annealed at 900 °C is shown in Fig. 1(b). Lattice parameters derived from the analysis are $a = 5.478(2)$ Å, $b = 7.735(3)$ Å, and $c = 5.508(2)$ Å for the sample annealed at 600 °C and $a = 5.472(1)$ Å, $b = 7.736(1)$ Å, and $c = 5.505(1)$ Å for this annealed at 900 °C. These lattice parameters are consistent with the literature data for similar ceramic samples.[23,25,26]

The average crystallite size $\langle D \rangle$ was calculated using Debye-Scherrer equation and was found to be 18 ± 1 nm for sample annealed at 600 °C and 70 ± 3 nm for this annealed at 900 °C. In the following text, the nanocrystalline samples with 18 and 70 nm average grain sizes will be referred to as 18 nm LCMO and 70 nm LCMO, respectively.

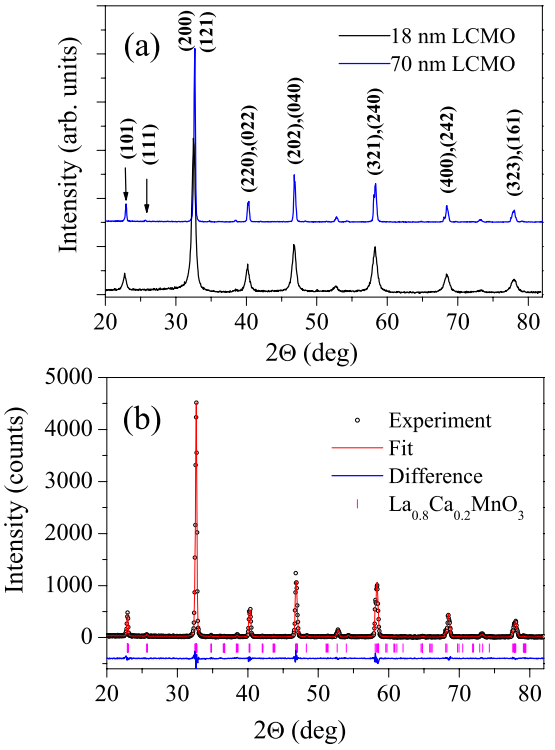

FIG. 1. (Color online) (a) XRD spectra of samples 18 nm LCMO and 70 nm LCMO annealed at 600 and 900 °C, respectively. Indexing is done in the orthorhombic setting of the *Pnma* space group; (b) Rietveld plot for 70 nm LCMO sample. The experimental data points are indicated by open circles, the calculated and difference patterns are shown by solid lines. The Bragg positions of the reflections of the orthorhombic manganite are indicated by vertical lines below the pattern.

The bright field TEM image of 18 nm LCMO powder dispersed in an alcohol and placed on a carbon grid is shown in Fig. 2(a). The powder is composed of nearly spherical nanoparticles with average size of 18 nm. The bigger particles appearing in the image were formed by aggregation of smaller particles in the process of preparation of the specimen for TEM. The SEM micrograph in Fig. 2(b) of the grinded surface of 18 nm LCMO pellet prepared for resistiv-

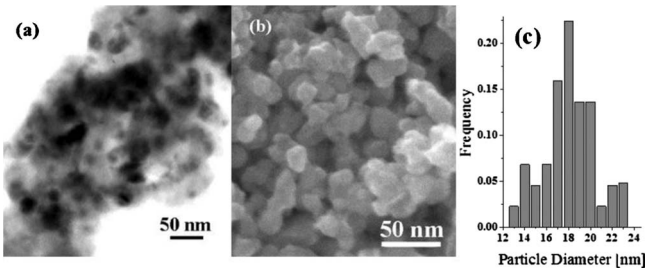

FIG. 2. (a) Bright field TEM image of 18 nm LCMO particles; (b) SEM image of the same sample after compacting into the pellet; (c) the normalized histogram of particle size distribution.

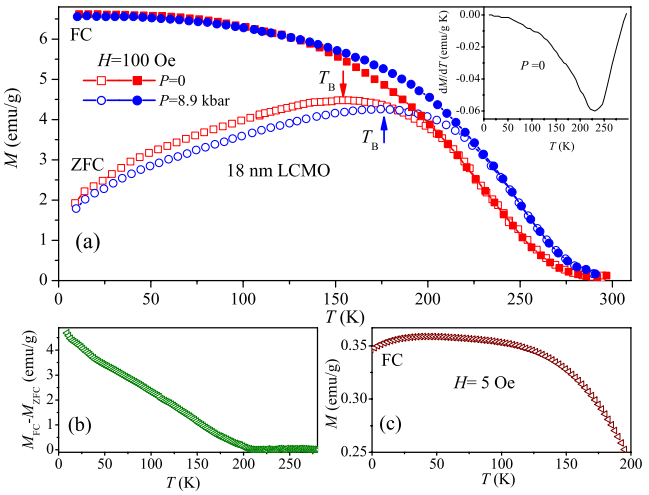

FIG. 3. (Color online) (a) Temperature dependence of zero-field cooled M_{ZFC} (open symbols) and field cooled M_{FC} (solid symbols) magnetization of 18 nm LCMO sample in magnetic field $H=100$ Oe at ambient pressure and at $P=8.9$ kbar. Inset shows temperature dependence of the derivative dM_{FC}/dT. (b) Difference between M_{FC} and M_{ZFC} as a function of temperature. (c) FC magnetization of 18 nm LCMO recorded in $H=5$ Oe in extended scale.

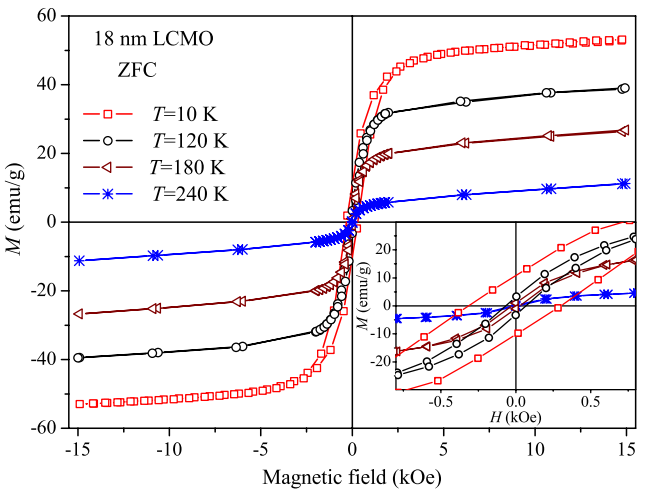

FIG. 4. (Color online) Magnetic field dependencies of magnetization of 18 nm LCMO sample measured after ZFC. Inset shows low-field part of hysteresis loops in the extended scale.

ity measurements shows a collection of almost uniform spherical nanoparticles. The normalized histogram of particle sizes computed from SEM micrographs is shown in Fig. 2(c). The average size obtained from this distribution agrees well with the one obtained using XRD data.

III. MAGNETIC AND TRANSPORT PROPERTIES

For magnetic measurements $La_{0.8}Ca_{0.2}MnO_3$ NP powders were compacted under pressure of ~5 kbar, applied at room temperature, into cylinder-shaped samples with diameter of 2.4 mm and height of 3.0 mm. Most of the magnetization measurements were conducted in the temperature range 5–290 K and magnetic field up to 15 kOe, applied perpendicularly to the rotation axis of a sample, employing a commercial vibrating sample magnetometer PAR 4500. The ac susceptibility was measured in the same temperature range using the magnetic option of the physical property measurement system of Quantum Design in which some of the magnetization measurements were also performed.

Temperature dependence of the field-cooled (M_{FC}) and zero-field-cooled magnetization (M_{ZFC}) of 18 nm LCMO sample is shown in Fig. 3. The curves were recorded at applied field of 100 Oe under ambient and at 8.9 kbar hydrostatic pressure. The temperature of the peak in $M_{ZFC}(T)$ curve can be associated with the blocking temperature T_B. At ambient pressure $T_B \approx 154$ K while at applied pressure of 8.9 kbar $T_B \approx 175$ K. For zero applied pressure, the Mn spin sublattice undergoes magnetic transition at Curie temperature $T_C \approx 231$ K, determined as the temperature of a minimum in the derivative of the magnetization curve $dM_{FC}(T)/dT$, see inset in Fig. 3(a). The magnetic transition is very broad due to some distribution of NP sizes and shapes in the ensemble, as well as due to interparticle and intraparticle magnetic interactions. The broadening of the magnetic transition is a characteristic feature of FM nanoparticle ensembles as demonstrated in studies of the grain size and oxygen stoichiometry influence on magnetic and transport properties of $La_{0.67}Ca_{0.33}MnO_3$ particles.[29] Therefore, the values of $T_C \approx 231$ K and $T_B \approx 154$ K should be understood as the average characteristic temperatures of the ensemble of 18 nm LCMO nanoparticles. Applied pressure increases T_C at a rate $dT_C/dP \approx 1.9$ K/kbar. At ambient pressure $M_{ZFC}(T)$ and $M_{FC}(T)$ curves diverge at the irreversibility temperature $T_{irr} \approx 208$ K, see Fig. 3(b), and the difference between them increases strongly with decreasing temperature. At low temperature M_{FC} saturates and becomes almost temperature independent. However, as it is shown in Fig. 3(c), M_{FC} recorded at very small magnetic field of 5 Oe initially increases slowly with decreasing temperature, almost saturates below 150 K, and starts to decrease at temperatures below 40 K.

Figure 4 shows the magnetization of 18 nm LCMO sample as a function of magnetic field applied at various temperatures after ZFC. Applied pressure does not practically change $M(H)$ curves. The nonlinearity in $M(H)$, indicating the onset of the ferromagnetism in the system, appears already at 240 K, significantly above T_C. Nonlinearity in $M(H)$ might be due to nonlinear nature of specific magnetic processes in the ensemble of 18 nm LCMO nanoparticles or, alternatively, may be related to the dispersion of particle size, Curie temperature, and anisotropy in the ensemble. The coercive field is relatively weak at temperatures slightly below T_C and monotonously increases with decreasing temperature, reaching 320 Oe at $T=10$ K, as seen in magnetic hysteresis loops in the inset in Fig. 4. The magnetization of 18 nm LCMO sample at 10 K remains unsaturated even at $H=15$ kOe, see Fig. 4. This is likely due to the superposition of contributions from FM particle core, which tends to saturate at low fields, and from magnetically disordered surface spins, which remain unsaturated at 15 kOe. The spontaneous magnetization M_0, obtained from a linear extrapolation of the high-field magnetization to $H=0$ was found to be M_0

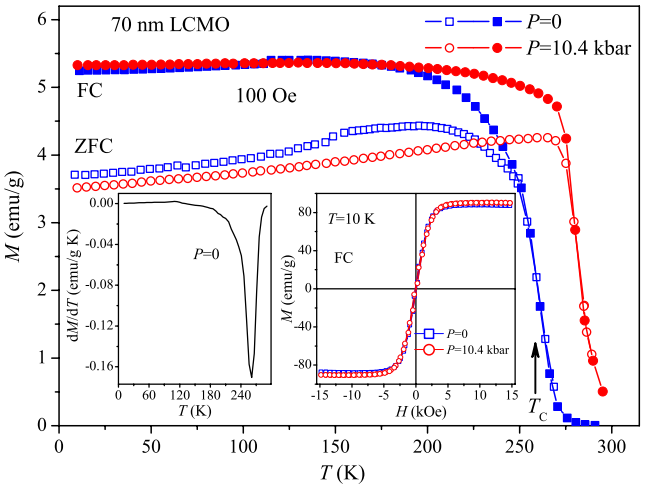

FIG. 5. (Color online) (a) Temperature dependence of zero-field-cooled M_{ZFC} (open symbols) and field-cooled M_{FC} (solid symbols) magnetization of 70 nm LCMO sample in magnetic field $H=100$ Oe at ambient pressure and at $P=10.4$ kbar. Left inset shows temperature dependence of the derivative dM_{FC}/dT. Right inset shows magnetic field dependencies of magnetization measured at $T=10$ K for 70 nm LCMO sample at ambient pressure and under $P=10.4$ kbar after FC.

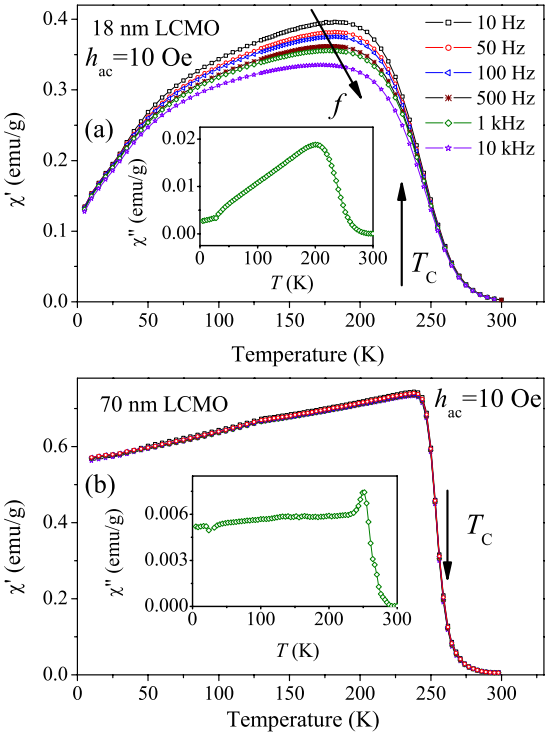

FIG. 6. (Color online) Temperature dependence of real component of ac susceptibility (χ') measured during heating, at different frequencies and ac magnetic field of 10 Oe for (a) 18 nm LCMO and (b) for 70 nm LCMO sample. Insets show the imaginary part (χ'') of ac susceptibility measured at frequency of 1 kHz and ac magnetic field of 10 Oe.

≈ 47.6 emu/g for 18 nm LCMO at 10 K, corresponding to the relative content of FM phase of 52%. Note that both, appearance of the peak in $M_{ZFC}(T)$ and $M(H)$ hysteresis below T_B are general characteristic features for magnetic nanosystems.[1–11]

The temperature dependence of M_{ZFC} and M_{FC} for 70 nm LCMO sample recorded in magnetic field of 100 Oe, at ambient pressure and at 10.4 kbar, is shown in Fig. 5. The difference between M_{ZFC} and M_{FC} below T_C is much smaller than in 18 nm LCMO case and magnetic transition at $T_C \approx 261$ K is significantly sharper, see left inset in Fig. 5. On the other hand, T_C increases with pressure with a rate $dT_C/dP \approx 1.8$ K/kbar, which is almost identical to that one of 18 nm LCMO, and similarly, the applied pressure does not practically affect $M(H)$ curves, see right inset in Fig. 5.

In contrast to behavior of $M(H)$ for 18 nm LCMO, the magnetization of 70 nm LCMO sample saturates in $H \sim 5$ kOe. Spontaneous magnetization of 70 nm LCMO at $T=10$ K is $M_0 \approx 87.6$ emu/g (right inset of Fig. 5), corresponding to the relative FM phase content of about 92%.

The temperature dependence of real part of ac susceptibility χ' was measured at several frequencies between 10 Hz and 10 kHz, with probing field amplitude of 10 Oe and temperature decreasing in short steps from 300 to 5 K. The ac susceptibility of 18 nm LCMO presented in Fig. 6(a) shows wide magnetic transition and significant frequency dependence in a wide temperature range below $T \sim 230$ K. In general, at all temperatures, χ' decreases with increasing frequency. The temperature T_p, at which the broad maximum in χ' appears, shifts to lower temperatures with increasing frequency and is equal to about 182 K at $f=10$ Hz while $T_p \approx 174$ K at $f=10$ kHz. This is a surprising and puzzling result since for both interacting and noninteracting NPs,[11,30,31] as well as for spin glasses,[22] the temperature of the peak in χ' is known to increase with increasing frequency. Most likely, the real evolution of the susceptibility of 18 nm LCMO is masked by effects of smeared FM ordering in the ensemble of NPs with some distribution of sizes, Curie temperature, and anisotropy field.

In a marked contrast, the susceptibility characteristics of 70 nm LCMO, shown in Fig. 6(b), resemble the behavior of ac susceptibility for conventional ferromagnets. In-phase component χ' exhibits an abrupt sharp increase in the vicinity of $T_C \sim 240$ K and only slight decrease with temperature decreasing below T_C. Very weak frequency dependence of the in-phase component, overall change of about 1.6% in the entire 10 Hz to 10 kHz frequency range, is seen only below T_C. There is some very small change in the slope of the temperature dependence of χ' around 140 K but the physics of this feature remains unclear at the moment. Out of phase component χ'' of ac susceptibility for both samples was found to be much smaller than real part χ' especially in low-temperature range and it also exhibits large scattering of experimental points particularly for curves recorded at low frequencies. Because of such large scattering we show in the insets in Figs. 6(a) and 6(b) representative curves of χ'' measured at $f=1$ kHz. In the inset in Fig. 6(a) we observe wide peak in the vicinity of T_C for 18 nm LCMO while for larger particles (70 nm LCMO) the peak is much sharper, see the inset in Fig. 6(b). Since $\chi''(T)$ affords the dissipated magnetic energy, the peak in $\chi''(T)$ should correspond to the irreversibility temperature T_{irr} at which the $M_{ZFC}(T)$ and $M_{FC}(T)$

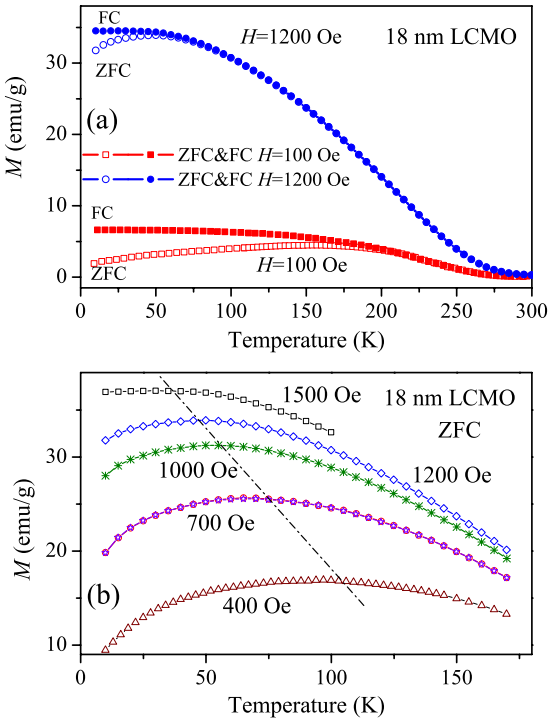

FIG. 7. (Color online) (a) Temperature dependence of zero-field-cooled M_{ZFC} (open symbols) and field-cooled M_{FC} (solid symbols) magnetization for 18 nm LCMO sample in magnetic field $H=100$ Oe and 1200 Oe; (b) M_{ZFC} recorded at various applied fields. The dotted line is a guide to the eye.

dependencies split below T_C.[32] Indeed, the temperatures of peaks in $\chi''(T)$ (201 K and 250 K for 18 nm LCMO and 70 nm LCMO, respectively) agree fairly well with the values of T_{irr}, see Figs. 3(a) and 5.

It is well known that in spin glasses the irreversibility temperature T_{irr} at which the $M_{ZFC}(T)$ and $M_{FC}(T)$ dependencies split depends strongly on the applied magnetic field.[33] Data presented in Fig. 7(a) prove that the same effect appears in our 18 nm LCMO sample. $T_{irr}(H)$ decreases progressively with increasing magnetic field until any noticeable difference between the ZFC and field-cooled (FC) magnetization vanishes at magnetic fields above 1500 Oe. Increasing magnetic field broadens and shifts the maximum of $M_{ZFC}(T)$ to lower temperatures, as illustrated in Fig. 7(b). The dotted line in Fig. 7(b) is a guide to the eye for the $M_{ZFC}(T)$ maximum position. This behavior indicates that with increasing field the magnetic energy becomes higher than the energy barrier between possible equilibrium orientations of magnetic moments, thereby decreasing both T_B and $T_{irr}(H)$.[34] Similar behavior, recently observed by Suzuki *et al.*[35] in ensembles of Fe_3O_4 NPs, was interpreted as a manifestation of a superspin-glass behavior.

Electrical resistance measurements were performed in a standard four-point arrangement using dc of 2 μA. Figure 8 shows the resistivity, recorded under zero magnetic field, as a function of temperature. Temperature dependence of resistivity for 70 nm LCMO demonstrates a clear insulator-to-metal transition at $T_{max} \approx 251$ K and quasimetallic $(dR/dT>0)$ behavior in a wide temperature range below T_{max}. In contrast, the resistivity of 18 nm LCMO monotonically increases with decreasing temperature and already at $T<150$ K becomes too large to be measured with our experimental setup.

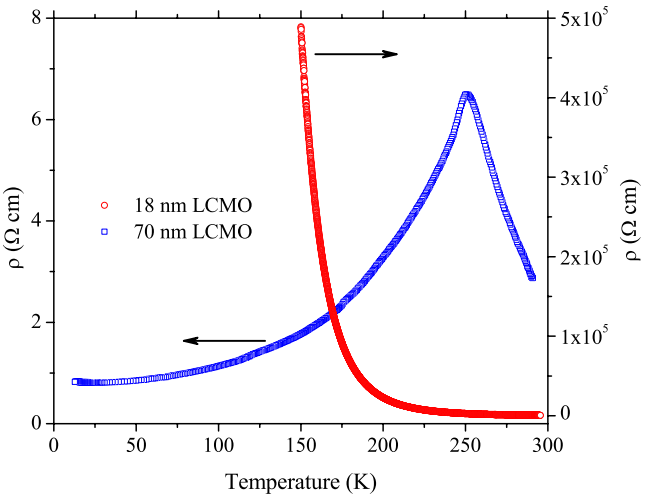

FIG. 8. (Color online) Resistivity ρ of 18 and 70 nm LCMO samples as a function of temperature.

IV. AGING, MEMORY, AND REJUVENATION EFFECTS

A characteristic feature of any glassy system, including SSG, is the aging effect in ZFC magnetization.[22,33] When magnetic field is applied to a glassy system which was cooled in zero field from a temperature above the glass temperature T_g to a temperature $T_w<T_g$, the time evolution of magnetization at T_w depends on the time spent by the system at low temperature before application of the field. In our experimental protocol the sample was cooled down to 100 K in zero magnetic field, maintained at low temperatures at $H=0$ for the waiting time t_w after which the magnetic field of 10 Oe was applied. The time evolution of magnetization resulting from slow relaxation is shown in Fig. 9(a). The observed time dependence of magnetization can be well approximated by a stretched exponential form[36]

$$M(t) = M_0 - M_g \exp[-(t/\tau)^{\beta}], \quad (1)$$

where M_0 is the magnetization of an intrinsic FM component while M_g is the initial magnetization of the glassy one, which provides the main contribution to the relaxation. The time constant τ and the dispersion parameter β are related to the relaxation rate of the spin-glass phase. The value of exponent β depends on the nature of energy barriers involved in the relaxation. For uniform energy barrier $\beta=1$ while for the system with distribution of energy barriers, what is typical for spin glasses, $0<\beta<1$. Fit of the stretched exponential Eq. (1) to the experimental data from Fig. 9(a) renders the following values of the fitting parameters: $\beta \approx 0.455$, 0.461, 0.446, $M_0=0.2049$, 0.2151, 0.1983 emu/g, $\tau=2602$, 2711, 3638 s, for t_w of 100, 1000, and 10 000 s, respectively. The results indicate a slow increase in time constant τ with increasing waiting time t_w.

In a generic aging process, the magnetization dependence on waiting time implies that the system is in a nonequilib-

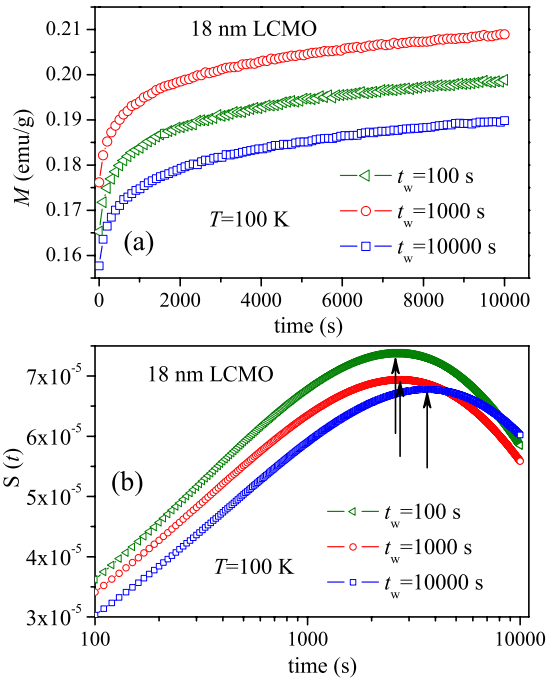

FIG. 9. (Color online) (a) Relaxation of ZFC magnetization of 18 nm LCMO at $T=100$ K for $t_w=100$, 1000, and 10 000 s; (b) Magnetic viscosity $S(t)=(1/H)dM(t)/d(\ln t)$ of 18 nm LCMO measured at 100 K for various waiting time. The curve for $t_w=1000$ s is shifted up by 0.2×10^{-5} to show better the position of maximum of $S(t)$.

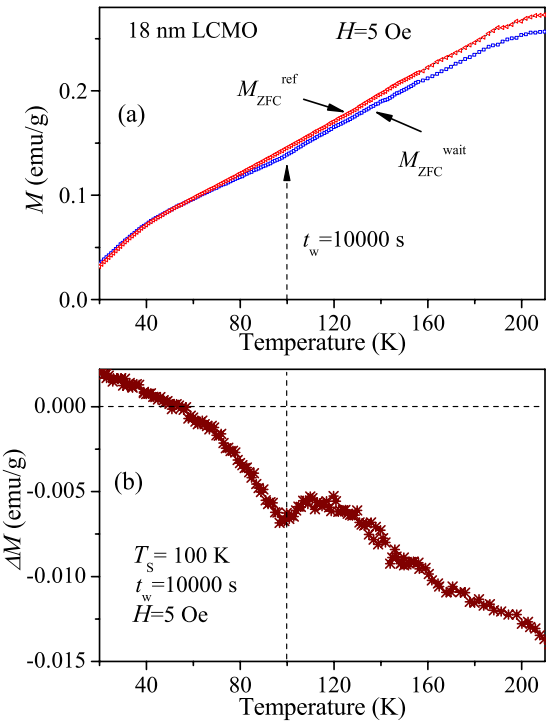

FIG. 10. (Color online) (a) Temperature dependence of the reference magnetization M_{ZFC}^{ref} (open triangles) and of the magnetization with a stop and waiting protocol, M_{ZFC}^{wait} (open squares) at a magnetic field $H=5$ Oe. First, 18 nm LCMO sample was cooled from 300 to 8 K with the rate of 5 K/min. Then magnetization was measured at heating, see M_{ZFC}^{ref}. After that the system was cooled again from 300 K to a stop temperature T_S. The system was annealed at stop temperature $T_S=100$ K for the wait time 10 000 s. The cooling was resumed from T_S to 8 K. Then the magnetic field was turned on and the magnetization M_{ZFC}^{wait} was measured at heating; (b) $\Delta M=M_{ZFC}^{wait}-M_{ZFC}^{ref}$ vs temperature.

rium state during t_w and that it keeps a memory of the waiting time after which field is applied. In classical SG systems, the time dependence of magnetization shows an inflection point at t_w, which is usually detected as a peak at $t\approx t_w$ in the magnetic viscosity $S(t)=(1/H)dM(t)/d(\ln t)$ plot versus t.[4,6,7,22,37–39] The effect is predicted for SG systems by the droplet model,[40] associating the maximum in magnetic viscosity $S(t)$ with a crossover from quasi-equilibrium dynamics at $t<t_w$ to nonequilibrium dynamics at $t>t_w$.

Time dependence of the magnetic viscosity $S(t)$ for 18 nm LCMO sample is shown in Fig. 9(b) for various t_w. In resemblance to classical SG systems,[22] the peak in the $S(t)$ shifts to longer times with increasing t_w, confirming the glassy magnetic behavior. However, in contrast to the behavior of classical SG systems and in some resemblance to the behavior of the $S(t)$ in polycrystalline $La_{0.6}Y_{0.1}Ca_{0.3}MnO_3$ manganites,[20] $La_{0.82}Sr_{0.18}CoO_3$ cobaltites,[41] and polymer-coated 7 nm magnetite NPs,[42] the waiting time dependence of the magnetic response in 18 nm LCMO is relatively weak. Note that the maximum of $S(t)$ moves only from 2600 to 3640 s upon three orders of magnitude changes in waiting time.

In order to investigate memory effects in ZFC magnetization we have employed a single stop-and-wait aging protocol. The sample was first ZFC cooled from room temperature down to 8 K at the rate of 5 K/min. The reference magnetization, M_{ZFC}^{ref}, was measured in magnetic field of $H=5$ Oe during reheating back to room temperature with the rate 0.5 K/min. In the next run the sample was cooled in zero magnetic field from 300 K to a stop point at $T_S=100$ K at the same cooling rate. The system was aged at T_S for $t_w=10\,000$ s. After the waiting time has elapsed, the ZFC was resumed and the sample cooled down to 8 K. At that temperature the magnetic field of $H=5$ Oe was turned on and M_{ZFC}^{wait} magnetization was measured again during the reheating cycle with the same heating rate 0.5 K/min as in M_{ZFC}^{ref} measurement. The temperature dependence of both M_{ZFC}^{ref} and M_{ZFC}^{wait} is shown in Fig. 10(a). Figure 10(b) demonstrates that the difference between M_{ZFC}^{wait} and M_{ZFC}^{ref} exhibits an aging dip in the vicinity of T_S. The dip results from spontaneous reconfigurations of magnetic moments toward the equilibrium state, through a growth of equilibrium domains at T_S. For systems with pure SG behavior, the reference and the stop-and-wait ZFC magnetization curves coincide at low and high temperatures and deviate only when the temperature T_S is approached from below.[7,36,37] However, in a difference to behavior of pure SG, our data show that splitting between M_{ZFC}^{wait} and M_{ZFC}^{ref} is not restricted only to the vicinity of T_S but persists also at temperatures below and above T_S. This is likely a result of only partial rejuvenation which is considered as a hallmark of the superspin-glass behavior of strongly interacting nanoparticles because the number of correlated superspins in SSGs in the experimental time scale is much smaller than in canonical atomic spin glasses. Rejuve-

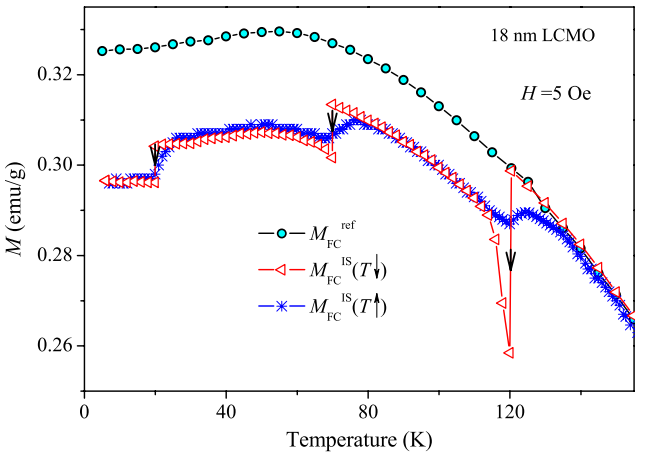

FIG. 11. (Color online) Temperature dependence of FC magnetization of 18 nm LCMO measured in the following protocol: M_{FC}, measured in magnetic field $H=5$ Oe, is defined as M_{FC}^{ref}. LCMO18 sample was FC cooled again from 300 K to intermittent stop temperatures $T_S=120$, 70, and 20 K, in $H=5$ Oe. At each T_S, the field was turned off and 18 nm LCMO was aged for a waiting time $t_w=1\times10^4$ s. Corresponding FC magnetization is denoted as $M_{FC}^{IS}(T\downarrow)$. The arrows point out the relaxation of $M_{FC}^{IS}(T\downarrow)$. $M_{FC}^{IS}(T\uparrow)$ is measured in $H=5$ Oe at increasing temperature after the above cooling.

nation effects involve a hierarchy of embedded active length scales what requires a large enough number of correlated spins in the system for the rejuvenation to be detectable. Therefore, rejuvenation effects in SSGs can be strongly reduced or even completely depressed.[43]

In the investigations of the memory effect in field cooled magnetization M_{FC} of 18 nm LCMO sample, we have adopted the methodology and definitions suggested recently by Suzuki *et al.*[35] According to the experimental protocol, the field-cooled reference magnetization $M_{FC}^{ref}(T)$ is measured in magnetic field $H=5$ Oe. Next, the sample is cooled down, in the same field, from 300 K to intermittent stop temperatures $T_S=120$, 70, and 20 K. At each T_S, the field is turned off and the system undergoes aging during the waiting time $t_w=1\times10^4$ s. While the system is aging at fixed temperature T_S, its magnetization $M_{FC}^{IS}(T\downarrow)$ decreases through relaxation, where IS stands for an intermittent stop. After the elapse of waiting time t_w, the magnetic field $H=5$ Oe is again turned on and the cooling is resumed. Such aging procedure leads to a steplike behavior of $M_{FC}^{IS}(T\downarrow)$ curve, as shown in Fig. 11. After reaching the final low temperature of 6 K the cooling is stopped and the magnetization is next measured with raising temperature $M_{FC}^{IS}(T\uparrow)$, in the presence of $H=5$ Oe during a continuous increase in the temperature at a constant rate of 0.5 K/min. Despite monotonic increase in the temperature in the heating run, $M_{FC}^{IS}(T\uparrow)$ undergoes step-like changes around each T_S, indicating that the system keeps a memory imprinted in the FC process.[12,13,35] The magnetization $M_{FC}^{IS}(T\downarrow)$ is almost parallel to the reference curve M_{FC}^{ref}, with exclusion of the temperatures around the intermittent stops T_S.

V. DISCUSSION

Densely packed ensembles of fine magnetic nanoparticles with strong interparticle interactions show most of the features which are characteristic of glassy systems.[4–7] Glassy behavior originates here from a complex interplay between surface and finite-size effects, interparticle interactions, and randomness of the distribution of anisotropy axes of nanoparticles. The values of the exchange coupling constants are expected to be different for individual interfaces and the form of their distribution may have a great influence on magnetic properties of the system.[14] The anisotropy of nanoparticles is somewhat related to slight deviations of their shapes from perfect spheres. Since all contributions act together, often with opposite effects, the glassy features are much less pronounced than in canonical spin glasses.[4]

FC magnetization memory is typical for SSG systems[8,12,33] and FC magnetization behavior very close to that one shown in Fig. 9 was recently observed in SSG ensembles of small 5 nm Fe_3O_4 NPs.[35] However, several papers show that superparamagnets may also exhibit similar memory effects.[9–13] A simple model of a noninteracting NPs, i.e., of a superparamagnetic system, as well as experimental investigations of superparamagnetic system, such as ferritin proteins, show that aging and memory effects may originate solely from a broad distribution of relaxation times arising from the anisotropy of energy barriers in paramagnets.[12] Indeed, FC magnetization memory was observed in various SPM systems such as γ-Fe_2O_3 NPs,[9] permalloy ($Ni_{81}Fe_{19}$),[8] and Co particles.[44]

In contrast, the memory effect in the ZFC magnetization is an unequivocal signature of SSG and in general of spin-glass behavior.[12] SPM should not exhibit any memory effect during ZFC below blocking temperature since the occupation probabilities of spin-up and spin-down states are always equal.[5] Moreover, the simultaneous decrease in M_{FC}^{ref} and $M_{FC}^{IS}(T\downarrow)$ in 18 nm LCMO is a common characteristic feature only for SSG and SFM systems because SPM systems exhibit a simultaneous increase in M_{FC}^{ref} and $M_{FC}^{IS}(T\downarrow)$.[8,12,13,35,44] This enable us to conclude at this point that aging and memory effects in 18 nm LCMO ensemble are not due to its SPM nature and result either from SSG or SFM nature of the system.

Unfortunately, waiting time-dependent magnetization relaxation appears in both SSG and SFM systems,[7] what does not allow us to discriminate between them. Investigations of magnetic relaxation of superferromagnetic granular multilayer $[Co_{80}Fe_{20}(1.4\ nm)/Al_2O_3(3\ nm)]_{10}$ have revealed two competing relaxations with different characteristic rates:[45] rapid relaxation of SFM domain walls and slow relaxation of superspins inside SFM domains toward higher colinearity against inherent random anisotropies.[7,45] SFM systems can also exhibit chaotic behavior similar to SSG, which may lead to relaxation, memory, and rejuvenation effects, through strong dependence of SFM order on temperature variation.[7,45]

Nevertheless, the waiting time dependence of the magnetic response in our samples is weaker than in archetypal spin glasses.[7] Thakur *et al.*[42] suggested that the relaxation processes in ensembles of magnetic NPs is due to combined effects of FM and SG components, what might cause the relaxation to deviate from a conventional SG behavior. We believe that sufficiently strong interactions in an ensemble of 18 nm LCMO particles result in formation of a collective

state and in an appearance of additional relaxation characteristic for SFM state. This in turn, modifies waiting time dependence and makes it different from that of conventional SG systems.

Other specific measurements should, in principle, allow one to distinguish between SSG and SFM behaviors. In particular, it was suggested that χ'' vs χ' Cole-Cole plot of SFM differs markedly from that of a SSG system.[6] Unfortunately, the Cole-Cole analysis of our data did not render any results that are different from those seen in both SSG and SFM systems. Possibly, it is related to a complex behavior of ac susceptibility and to absence of sufficiently pronounced glassy transition. We note that, a similar behavior has been already reported for $Y_{1-x}Ca_xMn_{1-y}Cr_yO_3$ ($x=0.3-0.4$) manganite system[46] and for low-Cr-doped manganite a transition from a typical spin-glass system to the nonuniform state with ferromagnetic clusters has been evidenced. In these experiments a number of features characteristic for spin glasses have been observed, nevertheless, the Cole-Cole analysis failed to reproduce the spin-glass behavior.[46]

Coexistence of nonequilibrium ferromagnetic and spin-glass components may modify dynamic characteristics of the system since both phases are in nonequilibrium states.[43,46] The system may exhibit magnetic aging and relaxation but typical characteristic features of canonical spin glasses, such as sharp dip of ZFC memory or appearance of maxima at t_w in $S(t)$ will be considerably less pronounced.[41,47,48]

The stability of spin-glass systems may be checked by the magnetic field dependence of their freezing temperatures. The real-space droplet theory[33] restricts SG correlations to so-called field crossover length, thus excluding appearance of long-range SG order in any magnetic field. On the other hand, the mean-field theory[48] predicts the existence of a critical de Almeida-Thouless (AT) line in the (H,T) plane. At low magnetic field AT line is given by

$$H(T) = H_0(1 - T/T_f)^p, \tag{2}$$

where T_f is the spin freezing temperature, H_0 is the magnetic field, and the exponent $p=3/2$. For Ising systems, the AT line directly separates the FM phase from the reentrant one with coexisting FM and SG orders. The behavior of ZFC magnetization maximum as a function of magnetic field in various materials is generally consistent with the AT line,[34] introduced originally for SG systems. In cluster glass models, ZFC magnetization peak is interpreted in terms of competition between randomly oriented moments of individual short-range clusters and the applied magnetic field.[31]

It was shown that temperature T_{max} of magnetic NPs ensembles with the spin disorder due to a surface spin-glass layer decreases with magnetic field following the $H^{2/3}$ dependence.[49,50] When the spin disorder extends to entire particle, T_{max} is expected to follow the $H^{1/2}$ dependence. In Fig. 12 we plot the temperature at which the maximum in $M_{ZFC}(T)$ appears (see Fig. 7) as a function of magnetic field. Fit of Eq. (2) to our experimental data yields $p=1.89\pm0.56$, $T_f=T_{max}=188\pm31$ K, and $H_0=2012\pm136$ Oe. Thus determined exponent p is close to the AT value of 1.5, indicating possible existence of AT critical line in the H-T phase diagram. On the other hand, the experimentally determined exponent $p=1.89\pm0.56$ is close to both $p=3/2$ and $p=2$, predicted by the theory for surface and volume spin disorder, respectively, what makes difficult to decide whether or not the system behaves as a re-entrant spin glass.[51] However, taking into account the fact that FM phase occupies only about 50% of the sample volume, we can deduce that the remaining half of the sample volume is occupied by the spin disordered phase. For 18 nm particles, half of the volume is occupied by surface shells of the thickness of about 2 nm. We conclude, therefore, that spin disorder is associated with surfaces and it is reasonable to assume that this increases the value of p toward 2. Recently, very similar AT critical line was obtained from the field dependence of the ZFC ac-susceptibility peak for 5 nm Fe_3O_4 NPs ensembles.[35] This system exhibits number of features characteristic for SSG such as aging, memory effects, and temperature independent M_{FC} at low temperatures. With increasing field, the temperature of the peak of ZFC susceptibility of Fe_3O_4 NPs shifts toward lower temperatures following AT line with the exponent $p=1.78\pm0.26$.[35] Furthermore, parameter $p=3/2$ is not unique for spin-glass states but it can also arise from the superparamagnetic behavior.[52] Therefore, the set of data, including the frequency dependence of susceptibility and low-temperature FC magnetization, as well as ZFC memory measurements and aging phenomena, are helpful to identify a glassy state. Somewhat larger parameter p for 18 nm LCMO sample may indicate the presence of considerable surface spin disorder or, alternatively, some intermediate state between SSG and SFM, if the interparticle magnetic interactions are sufficiently strong.

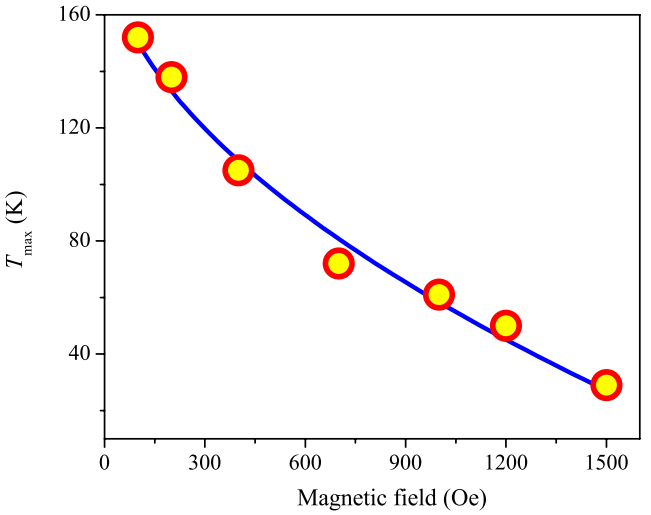

FIG. 12. (Color online) Temperature of the peak in ZFC magnetization as function of magnetic field for 18 nm LCMO particles. The solid line is fitted by Eq. (2) with following parameters: $T_f=188\pm31$ K; $H_0=2012\pm136$ Oe; and $p=1.89\pm0.56$.

Let us discuss the magnetic structure and the nature of interparticle interactions in ensembles of small manganite NPs. In order to explain magnetic properties of manganite NPs with sizes in the range of tens of nanometer, a core-shell structure was proposed.[53] The model assumes that the inner part of a particle, the core, has the same properties as the bulk material, whereas most of oxygen faults and vacancies

in the crystallographic structure are contained in the outer shell of the width t and constitute a magnetically dead layer (MDL). Recent magnetic and high-resolution TEM studies of 25 nm diameter $La_{0.67}M_{0.33}MnO_3$ (M=Ca,Sr) NPs have revealed the existence of 2 nm thick shells with properties different from those of the core.[54] Curiale *et al.*[54] demonstrated that atoms in the shells are arranged in a noncrystalline arrays, what explains 50% reduction in the surface magnetization with respect to the bulk. This is in a good agreement with the relative volume occupied by the FM in 18 nm LCMO. We claim that 18 nm LCMO NPs have FM cores surrounded by 2 nm thick surface MDL with crystalline and magnetic disorder. Curiale *et al.*[54] proposed that the MDL consists of small FM clusters containing just tens of Mn ions in a frustrated configuration that may result in appearance of a spin-glass-like layers at NPs surfaces.

We have previously established that due to the different nature of magnetic interactions in bulk $La_{1-x}Ca_xMnO_3$ below and above the percolation threshold x_C, the pressure coefficient dT_C/dP exhibits a sharp change in the vicinity of x_C and varies only slightly with doping increasing up to $x \sim 0.3$.[55] In the case of $x > x_C$, FM double exchange (DE) interactions control the magnetic and transport properties, whereas at $x < x_C$ DE is partly replaced by superexchange (SE) FM interactions. Double exchange is more sensitive to the pressure than SE and therefore the pressure coefficients are significantly different: $dT_C/dP \approx 0.2-0.3$ K/kbar and $dT_C/dP \approx 2$ K/kbar for $x < x_C$ and $x > x_C$, respectively.[55] Since the pressure coefficient $dT_C/dP \approx 1.8-1.9$ K/kbar is very close for our NPs ensembles to that of metallic $La_{1-x}Ca_xMnO_3$ ($x > x_C$) bulk manganites it seems reasonable to assume that a dominant magnetic interaction in the NPs cores is the ferromagnetic DE.

For all fine-particle systems, different interparticle interactions exist and play a decisive role in formation of collective states and determine magnetic behavior of NP ensembles. At higher particle densities, apart from the classical dipole interactions,[6,7] the exchange and other nonclassical interactions, such as tunneling exchange interactions, Ruderman-Kittel-Kasuya-Yosida, superexchange interactions, start to play a role in the system.[7] The evaluation of dipolar energy of interaction between two particles with moments $\mu = 3000\mu_B$ and a center-to-center distance of $D = 6$ nm will be $E_{d\text{-}d}/k_B = (\mu_0/4\pi k_B)(\mu^2/D^3) = 26$ K.[6,7] Taking into account all neighbors, the mean dipolar energy may increase to ~ 100 K.[6,7] It appears that dipole-dipole coupling may account for formation of collective states in ensembles of small NPs at $T \sim 100$ K. Taking into account the size and core-shell structure of 18 nm LCMO particles, we estimate μ to be $\sim 20\,000\mu_B$, giving rise to $E_{d\text{-}d}/k_B$ of ~ 45 K and the mean dipolar energy ~ 180 K. Analogous evaluation made for 70 nm LCMO particles gives even larger values: $E_{d\text{-}d}/k_B$ of ~ 80 K and the mean dipolar energy of about 320 K.

FM nanoparticles interacting only through dipolar interactions tend to create glassy disorder at high enough densities, while the formation of SFM state requires additional exchange-like interparticle interactions.[56,57] At high densities of particles, when their shells are in strong direct contact, the effective thickness of a shell is doubled and the exchange coupling interactions between atoms from neighboring particles start to play a role in the system along with classical dipole ones.[57]

Additional magnetic interparticle interaction, which may significantly contribute to the formation of collective SSG or SFM states in NP manganite ensembles, arises from the mechanism recently proposed by Rozenberg *et al.*[58] It was suggested that electrons tunneling between two Mn ions located in adjacent manganite NPs may induce FM DE correlations due to local spin polarization of these electrons, similarly to electron hopping between two Mn ions in the bulk. The DE correlations across the interface between two NPs are likely to be even stronger than the bulk counterpart due to dangling of some of Mn-O-Mn bonds on the grain surfaces.[58] Consequently, the FM-correlated spin clusters appear at the contact interfaces between neighboring grains. Spatial frustration of NPs in an ensemble results in randomization of FM moments and formation of SPM-like phase at temperatures $T > T_C$. Upon cooling toward T_C this effect starts to compete with the FM ordering in the cores and, as a result, the SPM-like electron magnetic-resonance signal becomes unobservable below T_C (Ref. 58) due to formation of the collective SFM-like state.

In the frame of the core-shell model individual FM nanoparticles consist of a FM core with collinear spin configuration and spin-glass-like shell with disordered spin configuration.[53,54] It should be underlined that the precise nature of the surface shell contribution remains unclear, what is well reflected in variety of terms used to describe its properties, such as, "disordered surface state," "uncoupled spins," or "spin-glass-like behavior."[59] High-resolution TEM investigations show that magnetically dead layer (shell) of $La_{0.67}X_{0.33}MnO_3$ (X=Ca,Sr) nanoparticles with a mean diameter of about 25 nm is approximately 2 nm thick.[54] It was proposed that ~ 2 nm thick surface shell has an internal structure containing small FM clusters, in form of 1.2 nm side cubes embracing four Mn ions, in *frustrated configuration*. Typically, the thickness of the surface layer, which has magnetic properties that are different from properties of the core, decreases with increase in the particle size.[60–62] Therefore spin-glass-like properties completely disappear in large particles. Experiments of Zhu *et al.*[62] confirm that pronounced spin-glass-like features in FM $La_{2/3}Sr_{1/3}MnO_3$ nanoparticles well seen for 25 nm particles, completely disappear when the particles size exceeds 50 nm. Our observations of the absence of spin-glass features in 70 nm LCMO particles are consistent both with the core-shell model predictions and results of known experiments. We conclude that significant surface spin-glass shell contribution together with strong interparticle interactions are vital prerequisites for appearance of SSG/SFM in ensembles of manganite nanoparticles.

Magnetic state and the phase diagram of dense ensembles of FM nanoparticles embedded in $[Co_{80}Fe_{20}(t_n)/Al_2O_3(3\text{ nm})]_{10}$ multilayers were recently investigated[56] as a function of the nominal thickness t_n using x-ray photoemission electron microscopy and magneto-optical Kerr microscopy. With increasing t_n the system shows first the SPM state at $t_n \leq 0.5$ nm, followed by the SSG behavior for $0.5 < t_n < 1.1$ nm, and the SFM state at 1.1 nm $\leq t_n \leq 1.8$ nm. Finally, percolated three-dimensional

ferromagnetism along with the Ohmic conduction develops above the physical percolation threshold at $t_n \approx 1.8$ nm. The conclusion is that in the SFM state FM long-range order, referred to as "magnetic percolation," is already well established even if the "physical percolation" and corresponding metallic conductivity is still absent.[56]

We suggest that magnetic state of ensembles of FM $La_{1-x}Ca_xMnO_3$ nanoparticles evaluates with increasing particle size in the way very similar to that described above. We propose that 18 nm LCMO shares properties of both SSG and SFM systems while the behavior of 70 nm LCMO particles is similar to a three-dimensional ferromagnetic with Ohmic conduction corresponding to the physical percolation.

VI. CONCLUSIONS

The results presented in this paper allow to conclude that magnetic and transport properties of LCMO NP ensembles with distinct particle sizes are in many aspects different. The magnetization of 18 nm LCMO is unsaturated at low temperatures while the resistivity has a semiconducting-like character. Furthermore, 18 nm LCMO exhibits strong frequency-dependent ac susceptibility, aging, and memory effects in wide temperature range allowing to conclude that below T_C a collective state is formed in ensembles of 18 nm LCMO particles. The collective state involves both spin-glass-like and nonequilibrium FM components and their interaction results in specific dynamic of the observed phenomena. In contrast to this behavior, the magnetization of 70 nm LCMO saturates at low temperatures while the resistivity exhibits well pronounced metallic-like behavior below T_C. Moreover, ensembles of larger particles do not show characteristic spin-glass features and their magnetic and transport characteristics resemble rather those bulk FM $La_{1-x}Ca_xMnO_3$ manganites with $x > x_C$ (percolation threshold).

The aging and memory effects, studied in series of dc magnetization measurements for 18 nm LCMO NPs using various cooling protocols, show the waiting time dependence in the magnetization relaxation due to a field change after ZFC. Nevertheless, clear waiting time dependence of ZFC relaxation is significantly weaker than that in canonical SG and SSG systems. The FC magnetization recorded with intermittent stop-and-wait method exhibits a step-like increase, at each stop temperature 20, 70, and 120 K, in reheating cycle. The genuine ZFC magnetization after ZFC procedure with single intermittent stop-and-wait event shows an aging dip at the stop temperature on the reheating. The flatness and even weak decrease in FC magnetization is observed for 18 nm LCMO below ZFC peak temperature. The ZFC-peak temperature monotonously decreases with increasing magnetic field, forming critical line with an exponent $p = 1.89 \pm 0.56$ in rough agreement with the de Almeida-Thouless exponent ($p = 3/2$). All results suggest the formation of collective state in ensemble of interacting 18 nm LCMO NPs with superspin-glass features developing together with superferromagnetic-like ones.

ACKNOWLEDGMENTS

This work was supported in part by the Polish Ministry of Science and Higher Education under a research Project No. N N202 1037 36 and by the Israeli Science Foundation administered by the Israel Academy of Sciences and Humanities under Grant No. 754/09.

*Corresponding author; markoviv@bgu.ac.il

[1] J. L. Dormann, D. Fiorani, and E. Tronc, Adv. Chem. Phys. **98**, 283 (1997).
[2] L. Néel, Ann. Geophys. (C.N.R.S.) **5**, 99 (1949).
[3] W. F. Brown, Jr., Phys. Rev. **130**, 1677 (1963).
[4] X. Batlle and A. Labarta, J. Phys. D **35**, R15 (2002).
[5] P. E. Jönsson, Adv. Chem. Phys. **128**, 191 (2004).
[6] O. Petracic, X. Chen, S. Bedanta, W. Kleemann, S. Sahoo, S. Cardoso, and P. P. Freitas, J. Magn. Magn. Mater. **300**, 192 (2006).
[7] S. Bedanta and W. Kleemann, J. Phys. D **42**, 013001 (2009).
[8] Y. Sun, M. B. Salamon, K. Garnier, and R. S. Averback, Phys. Rev. Lett. **91**, 167206 (2003).
[9] G. M. Tsoi, L. E. Wenger, U. Senaratne, R. J. Tackett, E. C. Buc, R. Naik, P. P. Vaishnava, and V. Naik, Phys. Rev. B **72**, 014445 (2005); G. M. Tsoi, U. Senaratne, R. J. Tackett, E. C. Buc, R. Naik, P. P. Vaishnava, V. M. Naik, and L. E. Wenger, J. Appl. Phys. **97**, 10J507 (2005).
[10] R. K. Zheng, H. Gu, B. Xu, and X. X. Zhang, Phys. Rev. B **72**, 014416 (2005).
[11] T. Jönsson, P. Nordblad, and P. Svedlindh, Phys. Rev. B **57**, 497 (1998); M. F. Hansen, T. Jönsson, P. Nordblad, and P. Svedlindh, J. Phys.: Condens. Matter **14**, 4901 (2002).
[12] M. Sasaki, P. E. Jönsson, H. Takayama, and P. Nordblad, Phys. Rev. Lett. **93**, 139701 (2004); M. Sasaki, P. E. Jönsson, H. Takayama, and H. Mamiya, Phys. Rev. B **71**, 104405 (2005).
[13] M. Bandyopadhyay and S. Dattagupta, Phys. Rev. B **74**, 214410 (2006).
[14] S. Mørup, M. B. Madsen, J. Franck, J. Villadsen, and C. J. W. Koch, J. Magn. Magn. Mater. **40**, 163 (1983).
[15] D. G. Rancourt and J. M. Daniels, Phys. Rev. B **29**, 2410 (1984).
[16] J. Tao, D. Niebieskikwiat, M. B. Salamon, and J. M. Zuo, Phys. Rev. Lett. **94**, 147206 (2005).
[17] Y. Yuzhelevski, V. Markovich, V. Dikovsky, E. Rozenberg, G. Gorodetsky, G. Jung, D. A. Shulyatev, and Ya. M. Mukovskii, Phys. Rev. B **64**, 224428 (2001).
[18] F. Rivadulla, M. A. López-Quintela, and J. Rivas, Phys. Rev. Lett. **93**, 167206 (2004).
[19] D. Niebieskikwiat, J. Tao, J. M. Zuo, and M. B. Salamon, Phys. Rev. B **78**, 014434 (2008).
[20] R. S. Freitas, L. Ghivelder, F. Damay, F. Dias, and L. F. Cohen, Phys. Rev. B **64**, 144404 (2001).
[21] E. Dagotto, *Nanoscale Phase Separation and Colossal Magnetoresistance*, Springer Series in Solid State Physics (Springer-Verlag, Berlin, 2003).
[22] J. A. Mydosh, *Spin Glasses* (Taylor & Francis, London, 1993).

[23] G. Biotteau, M. Hennion, F. Moussa, J. Rodriguez-Carvajal, L. Pinsard, A. Revcolevschi, Y. M. Mukovskii, and D. Shulyatev, Phys. Rev. B **64**, 104421 (2001).

[24] G. Papavassiliou, M. Belesi, M. Fardis, and C. Dimitropoulos, Phys. Rev. Lett. **87**, 177204 (2001); G. Papavassiliou, M. Pissas, M. Belesi, M. Fardis, J. Dolinsek, C. Dimitropoulos, and J. P. Ansermet, *ibid.* **91**, 147205 (2003).

[25] V. Markovich, E. Rozenberg, A. I. Shames, G. Gorodetsky, I. Fita, K. Suzuki, R. Puzniak, D. A. Shulyatev, and Y. M. Mukovskii, Phys. Rev. B **65**, 144402 (2002); V. Markovich, I. Fita, R. Puzniak, M. I. Tsindlekht, A. Wisniewski, and G. Gorodetsky, *ibid.* **66**, 094409 (2002); V. Markovich, G. Jung, Y. Yuzhelevski, G. Gorodetsky, A. Szewczyk, M. Gutowska, D. A. Shulyatev, and Ya. M. Mukovskii, *ibid.* **70**, 064414 (2004).

[26] M. Pissas, G. Papavassiliou, E. Devlin, A. Simopoulos, and V. Likodimos, Eur. Phys. J. B **47**, 221 (2005).

[27] D. Markovic, V. Kusigerski, M. Tadic, J. Blanusa, M. V. Antisari, and V. Spasojevic, Scr. Mater. **59**, 35 (2008).

[28] J. Rodriguez-Carvajal, Physica B **192**, 55 (1993).

[29] L. E. Hueso, F. Rivadulla, R. D. Sánchez, D. Caeiro, C. Jardón, C. Vázquez-Vázquez, J. Rivas, and M. A. López-Quintela, J. Magn. Magn. Mater. **189**, 321 (1998).

[30] S. D. Tiwari and K. P. Rajeev, Phys. Rev. B **72**, 104433 (2005).

[31] J. Wu and C. Leighton, Phys. Rev. B **67**, 174408 (2003).

[32] B. Roy, A. Poddar, and S. Das, J. Appl. Phys. **100**, 104318 (2006).

[33] K. H. Fischer and J. A. Hertz, *Spin Glasses* (University Press, Cambridge, 1991).

[34] M. K. Singh, R. S. Katiyar, W. Prellier, and J. F. Scott, J. Phys.: Condens. Matter **21**, 042202 (2009).

[35] M. Suzuki, S. I. Fullem, I. S. Suzuki, L. Wang, and C.-J. Zhong, Phys. Rev. B **79**, 024418 (2009).

[36] M. Ulrich, J. García-Otero, J. Rivas, and A. Bunde, Phys. Rev. B **67**, 024416 (2003).

[37] S. Sahoo, O. Petracic, W. Kleemann, P. Nordblad, S. Cardoso, and P. P. Freitas, Phys. Rev. B **67**, 214422 (2003).

[38] R. Mathieu, P. Jönsson, D. N. H. Nam, and P. Nordblad, Phys. Rev. B **63**, 092401 (2001).

[39] H. Mamiya, I. Nakatani, and T. Furubayashi, Phys. Rev. Lett. **80**, 177 (1998).

[40] D. S. Fisher and D. A. Huse, Phys. Rev. B **38**, 373 (1988); **38**, 386 (1988).

[41] Y. K. Tang, Y. Sun, and Z. H. Cheng, Phys. Rev. B **73**, 012409 (2006).

[42] M. Thakur, M. P. Chowdhury, S. Majumdar, and S. Giri, Nanotechnology **19**, 045706 (2008).

[43] P. E. Jönsson, H. Yoshino, H. Mamiya, and H. Takayama, Phys. Rev. B **71**, 104404 (2005); E. Wandersman, V. Dupuis, E. Dubois, R. Perzynski, S. Nakamae, and E. Vincent, EPL **84**, 37011 (2008); C. Raj Sankar, S. Vijayanand, S. Verma, and P. A. Joy, Solid State Commun. **141**, 307 (2007).

[44] R. K. Zheng, H. Gu, and X. X. Zhang, Phys. Rev. Lett. **93**, 139702 (2004).

[45] X. Chen, W. Kleemann, O. Petracic, O. Sichelschmidt, S. Cardoso, and P. P. Freitas, Phys. Rev. B **68**, 054433 (2003).

[46] D. Sedmidubský, J. Hejtmánek, M. Maryško, Z. Jirák, V. Hardy, and C. Martin, J. Appl. Phys. **91**, 8260 (2002); D. Sedmidubský, Z. Jirák, J. Hejtmánek, and M. Maryško, J. Magn. Magn. Mater. **272-276**, 1323 (2004).

[47] K. De, M. Patra, S. Majumdar, and S. Giri, J. Phys. D **40**, 7614 (2007).

[48] J. R. L. de Almeida and D. J. Thouless, J. Phys. A **11**, 983 (1978).

[49] H. Wang, T. Zhu, K. Zhao, W. N. Wang, C. S. Wang, Y. J. Wang, and W. S. Zhan, Phys. Rev. B **70**, 092409 (2004).

[50] H. Maletta and W. Zinn, in *Handbook on the Physics and Chemistry of Rare Earths*, edited by K. A. Gschneidner, Jr. and L. Eyring (North-Holland, Amsterdam, 1989), Vol. 12, p. 84.

[51] B. Martinez and X. Obradors, Ll. Balcells, A. Rouanet, and C. Monty, Phys. Rev. Lett. **80**, 181 (1998).

[52] L. E. Wenger and J. A. Mydosh, Phys. Rev. B **29**, 4156 (1984).

[53] M. A. López-Quintela, L. E. Hueso, J. Rivas, and F. Rivadulla, Nanotechnology **14**, 212 (2003); J. Rivas, L. E. Hueso, A. Fondado, F. Rivadulla, and M. A. López-Quintela, J. Magn. Magn. Mater. **221**, 57 (2000); L. E. Hueso, P. Sande, D. R. Miguéns, J. Rivas, F. Rivadulla, and M. A. López-Quintela, J. Appl. Phys. **91**, 9943 (2002).

[54] J. Curiale, M. Granada, H. E. Troiani, R. D. Sánchez, A. G. Leyva, P. Levy, and K. Samwer, Appl. Phys. Lett. **95**, 043106 (2009).

[55] V. Markovich, I. Fita, R. Puzniak, A. Wisniewski, K. Suzuki, J. W. Cochrane, Y. Yuzhelevskii, Ya. M. Mukovskii, and G. Gorodetsky, Phys. Rev. B **71**, 224409 (2005).

[56] S. Bedanta, T. Eimüller, W. Kleemann, J. Rhensius, F. Stromberg, E. Amaladass, S. Cardoso, and P. P. Freitas, Phys. Rev. Lett. **98**, 176601 (2007).

[57] M. F. Hansen, C. B. Koch, and S. Mørup, Phys. Rev. B **62**, 1124 (2000).

[58] E. Rozenberg, A. I. Shames, M. Auslender, G. Jung, I. Felner, J. Sinha, S. S. Banerjee, D. Mogilyansky, E. Sominski, A. Gedanken, Ya. M. Mukovskii, and G. Gorodetsky, Phys. Rev. B **76**, 214429 (2007).

[59] M. J. Benitez, O. Petracic, E. L. Salabas, F. Radu, H. Tüysüz, F. Schüth, and H. Zabel, Phys. Rev. Lett. **101**, 097206 (2008).

[60] Ll. Balcells, J. Fontcuberta, B. Martínez, and X. Obradors, Phys. Rev. B **58**, R14697 (1998).

[61] P. Dey and T. K. Nath, Phys. Rev. B **73**, 214425 (2006).

[62] T. Zhu, B. G. Shen, J. R. Sun, H. W. Zhao, and W. S. Zhan, Appl. Phys. Lett. **78**, 3863 (2001).